

# Journal of Materials Chemistry B

Materials for biology and medicine

Accepted Manuscript

This article can be cited before page numbers have been issued, to do this please use: H. Han, D. Lee, A. Joe, Y. J. Jeon, Y. Lim, S. B. Lee, B. Bin, J. Lee, T. Thambi, J. Conde, M. Panchanathan and E. Jang, *J. Mater. Chem. B*, 2026, DOI: 10.1039/D6TB00534A.



This is an Accepted Manuscript, which has been through the Royal Society of Chemistry peer review process and has been accepted for publication.

Accepted Manuscripts are published online shortly after acceptance, before technical editing, formatting and proof reading. Using this free service, authors can make their results available to the community, in citable form, before we publish the edited article. We will replace this Accepted Manuscript with the edited and formatted Advance Article as soon as it is available.

You can find more information about Accepted Manuscripts in the [Information for Authors](#).

Please note that technical editing may introduce minor changes to the text and/or graphics, which may alter content. The journal's standard [Terms & Conditions](#) and the [Ethical guidelines](#) still apply. In no event shall the Royal Society of Chemistry be held responsible for any errors or omissions in this Accepted Manuscript or any consequences arising from the use of any information it contains.

1 **Wearable near-infrared LED photothermal microneedle patch reduces**  
2 **periorbital wrinkles in a randomized pilot clinical trial**

3  
4 Hyo-Won Han,<sup>a, 1</sup> Dong-Hwan Lee,<sup>b, 1</sup> Ara Joe,<sup>a</sup> Yeong Jun Jeon,<sup>c</sup> Yu-Ra Lim,<sup>c</sup> Sang Bong Lee,<sup>d</sup> Bum-  
5 Ho Bin,<sup>b</sup> JuKyung Lee,<sup>e</sup> Thavasyappan Thambi,<sup>f</sup> João Conde,<sup>g,\*</sup> Panchanathan Manivasagan,<sup>c,\*</sup> and Eue-  
6 Soon Jang <sup>a, c, \*</sup>

7  
8 <sup>a</sup> Golden Crow Co., Ltd., Global building #140, Daehak-ro 61, Gumi, Gyeongbuk 39177, Republic of  
9 Korea

10 <sup>b</sup> Department of Applied Biology, Ajou University, Kyonggi-do, Republic of Korea, and 206, Worldcup-  
11 ro, Yeongtong-gu, Suwon-si, Gyeonggi-do, 16499, Republic of Korea

12 <sup>c</sup> Department of Chemistry and Bio Science, Kumoh National Institute of Technology, Daehak-ro 61,  
13 Gumi, Gyeongbuk 39177, Republic of Korea

14 <sup>d</sup> Department of Nursing, Chung Cheong University, Cheongju, Chungbuk, Republic of Korea

15 <sup>e</sup> Digital Health Care Research Center, Gumi Electronics and Information Technology Research Institute  
16 (GERI), Gumi, Gyeongbuk 39253, Republic of Korea

17 <sup>f</sup> Graduate School of Biotechnology, College of Life Sciences, Kyung Hee University, Yongin-si,  
18 Gyeonggi-do 17104, Republic of Korea

19 <sup>g</sup> Comprehensive Health Research Centre (CHRC), NOVA Medical School, Faculdade de Ciências  
20 Médicas, NMS|FCM, Universidade NOVA de Lisboa, Lisboa, Portugal

21



22 \* Corresponding authors: [euesoon@kumoh.ac.kr](mailto:euesoon@kumoh.ac.kr) (E.-S.J.) ; [manimaribtech@gmail.com](mailto:manimaribtech@gmail.com) (P.M.) and  
23 [joao.conde@nms.unl.pt](mailto:joao.conde@nms.unl.pt) (J.C.)

24 <sup>1</sup> These authors contributed equally.

## 25 26 **ABSTRACT**

27 Microneedle patches are typically passive, limiting control over dissolution kinetics and transdermal  
28 transport. Here we introduce a wearable, actively actuated microneedle system in which dissolving  
29 hyaluronic-acid tips penetrate the stratum corneum while a hydrocolloid backing embedded with  
30 hyaluronic-acid-gold-nanorod (HA-GNR) nanocomposites provides near-infrared (NIR,  $\approx 780$  nm)  
31 photothermal actuation. Under brief LED illumination, the GNRs deliver a mild, eyelid-safe thermal  
32 micro-dose ( $\sim 41$  °C) that accelerates tip dissolution and enhances short-range transport without increasing  
33 needle length. Tissue-mimicking phantoms show heat-augmented dye advance ( $\approx 5.1$  mm vs  $\approx 2.6$  mm at  
34 15 min), supporting a mechanism involving accelerated dissolution and enhanced localized transport  
35 driven by combined diffusion and micro-convective effects. In a monocentric, randomized, investigator-  
36 blinded pilot trial (n=20 women, 30–59 yr) with thrice-weekly use for four weeks, under-eye PRIMOS  
37 average roughness (Ra) improved by 16.3% at week 4 ( $p < 0.001$ ), and periorbital brightness (VISIA-CR  
38 L\*) increased by  $\sim 1.5$ – $2.0\%$ . A with-/without-NIR comparison at the crow's-feet favored actuation ( $\sim 14.1\%$   
39 vs  $\sim 1.9\%$  improvement at week 4). No device-related adverse events were observed. By decoupling  
40 penetration from actuation through a plasmonic nanocomposite backing, this platform transforms  
41 dissolving microneedles into programmable, eyelid-compatible transdermal devices with human evidence,  
42 suggesting broad utility for gentle, controllable delivery at sensitive sites.



43 **Keywords:** Hyaluronic acid; gold nanorods; microneedle patch; photothermal therapy; periorbital  
44 wrinkles; clinical trial.

45

## 46 1. Introduction

47 Skin aging is a prominent indicator of physical age,<sup>1</sup> with periorbital skin being the most susceptible given  
48 that it is the thinnest part of the face.<sup>2</sup> The eye is the most sensitive and fragile region of the skin.<sup>3</sup> Aging,  
49 lack of sleep, daily stress, radiation, smoking, and environmental pollutants contribute to the development  
50 of crow's feet and periorbital wrinkles, resulting in a tired appearance.<sup>4-6</sup> Filler injections are low-cost  
51 cosmetic treatments that involve the injection of a gel-like material under the skin to improve wrinkles or  
52 soft tissues.<sup>7</sup> However, intravascular filler injections can have serious side effects, including skin necrosis,  
53 visual loss, and facial overfilling syndrome.<sup>8-11</sup> The increasing demand for aesthetic medical procedures  
54 has recently sparked public interest in specialist consultations with dermatologists, resulting in an urgent  
55 need to develop an efficient, safe, and innovative at-home eye-wrinkle cosmetic product to satisfy  
56 customer demands and improve the quality of life.<sup>12</sup> Microneedle patches have emerged as a popular at-  
57 home anti-wrinkle product among the many anti-wrinkle cosmetic products available on the market (e.g.,  
58 creams, lotions, facial masks, moisturizers, and fabrics).<sup>13-16</sup>

59 Recently, microneedle patch technology has been increasingly used in the field of aesthetic  
60 medicine, given its advantages, such as painlessness, high safety, and ease of use. Furthermore, given the  
61 length and thickness of the needles, it can be used as a non-invasive home skin care device for treating  
62 wrinkles.<sup>2</sup> Microneedles are extremely small, submillimeter-sized needles arranged in an array to  
63 penetrate the outer skin layer.<sup>17-20</sup> Recently, a photothermal microneedle patch (PMP) that combines  
64 microneedle technology with photothermal therapy (PTT) has emerged as an innovative approach to  
65 improve periorbital wrinkles.<sup>21</sup> PMPs are composed of polymers and photothermal (PT) agents, including



66 hyaluronic acid (HA) and gold nanorods (GNRs). HA is a naturally occurring biopolymer consisting of  
67 repeating disaccharide units of D-glucuronic acid and N-acetyl-D-glucosamine, which are endogenous  
68 components of human skin and the extracellular matrix of human tissues.<sup>22</sup> HA is a versatile material with  
69 several unique properties, including water-binding capacity, swelling, biocompatibility, biodegradability,  
70 and safety, making it a suitable candidate for developing safe cosmetic products aimed at improving  
71 wrinkles, moisture, and elasticity in dermatology.<sup>23, 24</sup>

72 PTT has emerged as an effective therapeutic approach for treating cancer and microbial infections  
73 because of its noninvasiveness, ease of operation, high spatiotemporal resolution, high specificity, and  
74 low side effects.<sup>25</sup> PT materials are used to convert NIR light into heat energy (>43 °C) when exposed to  
75 external NIR light sources.<sup>26</sup> PT materials, such as GNRs, are most commonly used in PTT because of  
76 their unique properties, such as excellent biocompatibility, high PT conversion efficiency, easy synthesis,  
77 and high absorption in the NIR region, resulting in a better enhancement of PT heat generation to improve  
78 wrinkle appearance, create smoother skin, and achieve a more youthful appearance.<sup>27</sup> In recent years, PT  
79 microneedle systems have advanced rapidly for controlled drug administration, wound healing, and  
80 minimally invasive therapeutic applications have advanced rapidly in recent years, particularly through  
81 NIR-responsive platforms that allow fine spatiotemporal management of treatment effects.<sup>28-31</sup> However,  
82 photothermal agents are directly integrated into the microneedle matrix in most described systems, which  
83 may lead to uneven heat distribution and greater skin exposure to nanomaterials. Despite these  
84 developments, few studies have focused on the creation of safe, regulated, and user-friendly at-home PT  
85 microneedle systems, and their application in delicate cosmetic areas, such as the periorbital area, remains  
86 largely underexplored.<sup>32, 33</sup>

87 In this study, we developed the first PT-responsive soluble microneedle patch (PMP) as a novel  
88 emerging at-home cosmetic product for improving periorbital wrinkles (**Scheme 1**). The developed PMP



89 comprises cross-linked HA particulate-based needle tips and an HA-GNR-based hydrocolloid pad as the  
90 back surface. Notably, HA-based microneedle tips and the top of the thin film of the adhesive hydrocolloid  
91 pad were in direct contact with the skin, which did not have GNRs, and demonstrated that HA-GNRs were  
92 successfully fabricated on the back of the hydrocolloid pad. The fabricated PMP was applied horizontally  
93 under the eyes and vertically in the crow's feet region, and it was gently pressed for 5 s to reach the upper  
94 epidermis without pain, bleeding, redness, injury, or infection. A NIR light-emitting diode (LED) eye  
95 mask device (780 nm), worn over microneedle patches, ensures a safe temperature increase (41.0 °C) for  
96 eyelid warming; this reduces wrinkles, fine lines, and other signs of aging, while improving skin  
97 rejuvenation, tightening, elasticity, texture, collagen production, fibroblast activation, and dermal blood  
98 flow. Our results confirm that PMP with NIR LED light is a new, safe, and effective home-use cosmetic  
99 product for improving periorbital wrinkles and can become a highly valuable cosmetic product that can  
100 improve the quality of life in the future.

## 102 2. Materials and methods

### 103 2.1. Materials

104 Benzyltrimethylhexadecylammonium chloride (BDAC), Gold(III) chloride trihydrate ( $\text{HAuCl}_4 \cdot 3\text{H}_2\text{O}$ ),  
105 sodium borohydride ( $\text{NaBH}_4$ ), hexadecyltrimethylammonium bromide (CTAB), L-ascorbic acid, silver  
106 nitrate ( $\text{AgNO}_3$ ), agarose, methylene blue, sodium hydroxide ( $\text{NaOH}$ ), and 1,4-Butanediol diglycidyl ether  
107 (BDDE) were supplied by Sigma-Aldrich (USA). Hyaluronic acid (HA) was obtained from SK Bioland  
108 Co., Ltd. (Cheonan, Korea). Hibitane solution was supplied by Tokyo Kasei Kogyo Co., Ltd. (Tokyo,  
109 Japan). Ultrapure water was produced using an aquaMAX-Ultra 370 water purification system (YL  
110 Instrument Co., Ltd, Korea) and used in all experiments.

111



## 112 2.2. Clinical study design and participants

113 This prospective study was a monocentric, randomized, investigator-blinded, controlled pilot trial for  
114 investigating the efficiency and safety of a PMP system to treat periorbital wrinkles and crow's feet. This  
115 study was reviewed and approved by the Cutis Institutional Review Board of the Human Research Ethics  
116 Committee of the Cutis Biomedical Research Center (Seoul, Korea). All volunteers provided written  
117 informed consent and agreed to produce digital photographs before the study (Approval number: CBRC-  
118 E-211115-58). The volunteers were selected based on their ability to be monitored and followed during  
119 experiments. A total of 20 healthy Korean women aged 30–59 years were enrolled in this pilot study  
120 conducted between November 2021 and January 2022. All participants had mild-to-moderate periorbital  
121 wrinkles according to the wrinkles scale and sought aesthetic improvements in the facial region<sup>34</sup>. None  
122 of the participants had dermatologic diseases, were pregnant, or breastfed.

## 123 2.3. Photothermal microneedle patch (PMP)

124 The cross-linked HA particulate and PMP were designed and developed by Endoderma Co., Ltd.  
125 (Seongnam, Korea) as a fee-based service following their standardized industrial protocol. The synthesis  
126 method of the cross-linked HA particulate and their incorporation into microneedle structures follows the  
127 manufacturing protocol previously described by Choi et al.,<sup>35</sup> who developed the technology at  
128 Endoderma Co., Ltd. (Seongnam, Korea). The preparation of a PMP is based on a combination of  
129 microneedle technology and PTT using medical adhesive bandages. The PT microneedles were fabricated  
130 using the micromolding method and comprised cross-linked HA particulate-based needle tips and an  
131 adhesive hydrocolloid pad based on HA-GNRs. HA solutions with various concentrations were fabricated  
132 by combining the HA solution and cross-linked HA particulates at weight ratios of 20:80, 40:60, 60:40,  
133 80:20, and 100:0 in deionized water (DW) for preparing needle tips with different concentrations of cross-  
134 linked HA particles. Additionally, the mixed solution (2.5 mL) was added to the micromold and

135 centrifuged to fill the needle cavity, which was then dried at room temperature for 30 min. The prepared  
136 HA solution was first placed on top of a thin film of the adhesive hydrocolloid pad. Then, GNRs were  
137 prepared through the seed-mediated growth method reported in our previous work (Korean Patent  
138 “Preparation method of Au nanorod,” No: 10-1333962)<sup>27, 36-38</sup> and GNRs (75 parts per million of gold  
139 (ppm of Au)) embedded with the HA solution onto the adhesive back surface of the hydrocolloid pad from  
140 Endoderma Co., Ltd. (Seongnam, Korea)<sup>35</sup> through a fee-based manufacturing service according to this  
141 established protocol. After drying, the molds were peeled off to obtain PT microneedle arrays. To ensure  
142 stability, all patches were vacuum-packaged in moisture-impermeable foil pouches, a standard industrial  
143 process used for dissolving microneedle products. Vacuum packaging prevents water uptake and allows  
144 long-term storage at room temperature. The company announced that the cross-linked HA microneedle  
145 patch was registered and approved by the Food and Drug Administration (FDA) for cosmetic applications.  
146 This approved product does not include GNRs. The PMP employed in this study represents a research  
147 prototype, and regulatory approval for this modified version is currently being pursued. The fabrication  
148 process followed a standardized, previously validated protocol.<sup>35</sup> The physicochemical properties of cross-  
149 linked HA particulates, such as crosslinking behaviour, swelling characteristics, and degradation profiles,  
150 have been systematically reported in previous studies.<sup>35</sup> In the present study, we focused on the device-  
151 level fabrication and functional performance of the PMP system. To further strengthen reproducibility,  
152 additional batch-specific characterization of material properties will be included in future studies.

#### 153 2.4. Morphological analysis

154 The PMPs were visualized using a Leica S9i stereomicroscope (Leica Microsystems Co. Ltd., Deerfield,  
155 IL, USA) to investigate the morphology of the microneedles. The morphological properties and elemental  
156 distribution of the PMP were investigated using a field-emission scanning electron microscope (FE-SEM,  
157 JSM-IT700HR, JEOL, Japan) equipped with an energy-dispersive X-ray spectrometer (EDX).

158 Transmission electron microscopy (TEM, JEM2100, JEOL, Japan) was used to observe the surface  
159 morphology of the GNRs.

## 160 2.5. NIR LED light-responsiveness of the PMP

61 GNRs with varying concentrations (0, 0.1, 1, 5, 10, 30, 50, 75, 100, 150, 200, and 300 ppm of Au) were  
62 exposed to 785 nm NIR laser (CNI, MDL-III-785, Changchun, China) irradiation at 0.8 W/cm<sup>2</sup> for 30  
63 min. The PMP (75 ppm Au) and microneedle patch (0 ppm Au) were placed on a board of NIR LED  
64 lights (Epitex, SMBB780D-1100-03, Japan) at a wavelength of 780 nm and exposed to an NIR LED light  
65 source for 15 min. The temperature change curves of the PMP were recorded, and an infrared (IR) thermal  
66 imaging camera (FLIR CX-Series, Wilsonville, Oregon, USA) continuously captured the real-time  
67 temperature of the PMP.

## 68 2.6. Tissue-mimicking agarose gel phantom

69 Agarose gel phantoms for imaging were constructed using 1% agarose powder as the base material by  
70 dissolving it in 100 mL of DW. The agarose gel phantom was cylindrical with a diameter and height of 7  
71 and 9.5 mm, respectively. The top of the agarose gel phantom was embedded with or without HA-GNRs,  
72 and the diffusion process of methylene blue (MB) solution (10  $\mu$ L, 0.0125 g/mL) was added dropwise on  
73 the top of the agarose gel phantom.<sup>39, 40</sup> A high-power top NIR LED light with a peak wavelength of 780  
174 nm was obtained from Epitex (SMBB780D-1100-03, Japan). An NIR LED light (wavelength of 780 nm)  
175 was placed on the top surface of a phantom exposed to the NIR LED light for 15 min for visualizing the  
176 dye penetration depth in tissues because of the PT heat energy, which was observed and measured in the  
177 MB diffusion inside the agarose gel phantom.

## 178 2.7. Intervention

179 All participants washed their faces and rested at room temperature for 15 min, and were asked to clean  
180 their eyes with a hibitane solution and dry the test area well before applying PMP to the area under the

181 eyes and the crow's feet region. All participants were instructed to apply a PMP under the eyes, and a  
182 patch was gently pressed onto the under-eye region for 5 seconds, which ensured that the entire surface of  
183 the patch was in full contact with the skin for 5 min to enable the needle to penetrate deeply. A wearable  
184 NIR LED eye mask device (YOUR NEED79, model CG-001; Freewind, Korea) was used for clinical  
185 application. The device delivered NIR light with a peak wavelength of 780 nm ( $\pm 10\%$ ), corresponding to  
186 an emission range of approximately 702-858 nm, and operates in multiple modes. It is powered by a built-  
187 in rechargeable lithium-ion battery (7.2 V, 3350 mAh) with a maximum output of 20 W. A wearable NIR  
188 LED eye mask device was worn over microneedle patches, which were exposed to NIR LED light at 780  
189 nm for 15 min to generate mild heat (PT effect), followed by cooling at room temperature without NIR  
190 LED light for 15 min, and then by removing the NIR LED device and patches, whereas PMPs (control)  
191 was applied for the same total duration of 30 min without NIR LED light exposure. All participants  
192 received moisturizers and were instructed to apply PMPs with NIR LED light for 15 min, three times a  
193 week, for a total of four weeks. All participants visited the clinic weekly throughout the study.

## 2.8. Quantitative evaluation of wrinkle improvement

194  
195 Periorbital wrinkles, crow's feet wrinkles, and skin roughness were evaluated quantitatively using a small-  
196 field PRIMOS<sup>CR</sup> (Canfield Scientific Inc., USA) equipped with a non-contact optical three-dimensional  
197 (3D) skin imaging device, in which a decrease in  $R_a$  (average roughness) values indicates an improvement  
198 in wrinkles to measure wrinkle changes. The wrinkle changes in the left and right eyes and the crow's feet  
199 region were analyzed using wrinkle analysis parameters. Skin brightness was measured and captured using  
200 VISIA-CR (Canfield Scientific Inc., USA) at baseline and at every visit, offering a standard high-  
201 resolution facial photography device to identify subsurface skin characteristics. The images captured using  
202 VISIA-CR were analyzed using the image analysis software I-MAX Plus (INGPLUS Co., Ltd, Seoul,  
203 Korea) to designate the area around the eyes in which an increase in the  $L^*$  value indicates an improvement



204 in skin brightness. Images at the same site were captured at each evaluation time point (baseline (zero),  
205 two, and four weeks).

## 206 **2.9. Product preference and safety**

207 All participants were surveyed at every visit for adverse skin reactions, including burning, itching, scaling,  
208 prickling, redness, tightness, swelling, erythema, and edema. The efficacy and safety of the application  
209 were evaluated at the same site using the same methodology as that used at the initial visit at zero, one,  
210 two, and four weeks. In addition to participant-reported symptoms, safety assessments included  
211 dermatologist-performed visual examination at each visit to detect any signs of irritation or adverse skin  
212 reactions.

## 213 **2.10. Statistical analysis**

214 The statistical significance of all data was determined using SPSS version 27.0 (SPSS Inc., Chicago, IL,  
215 USA). All experiments were performed in at least triplicate ( $n \geq 3$ ) and data were expressed as mean  $\pm$   
216 standard deviation (SD), with the statistical significance set at  $p < 0.05$ . Comparison within the population  
217 was conducted using the non-parametric Friedman test (Post hoc: Wilcoxon signed rank test with  
218 Bonferroni correction), parametric test, and repeated-measures analysis of variance (ANOVA) (Post hoc:  
219 Bonferroni correction).

220

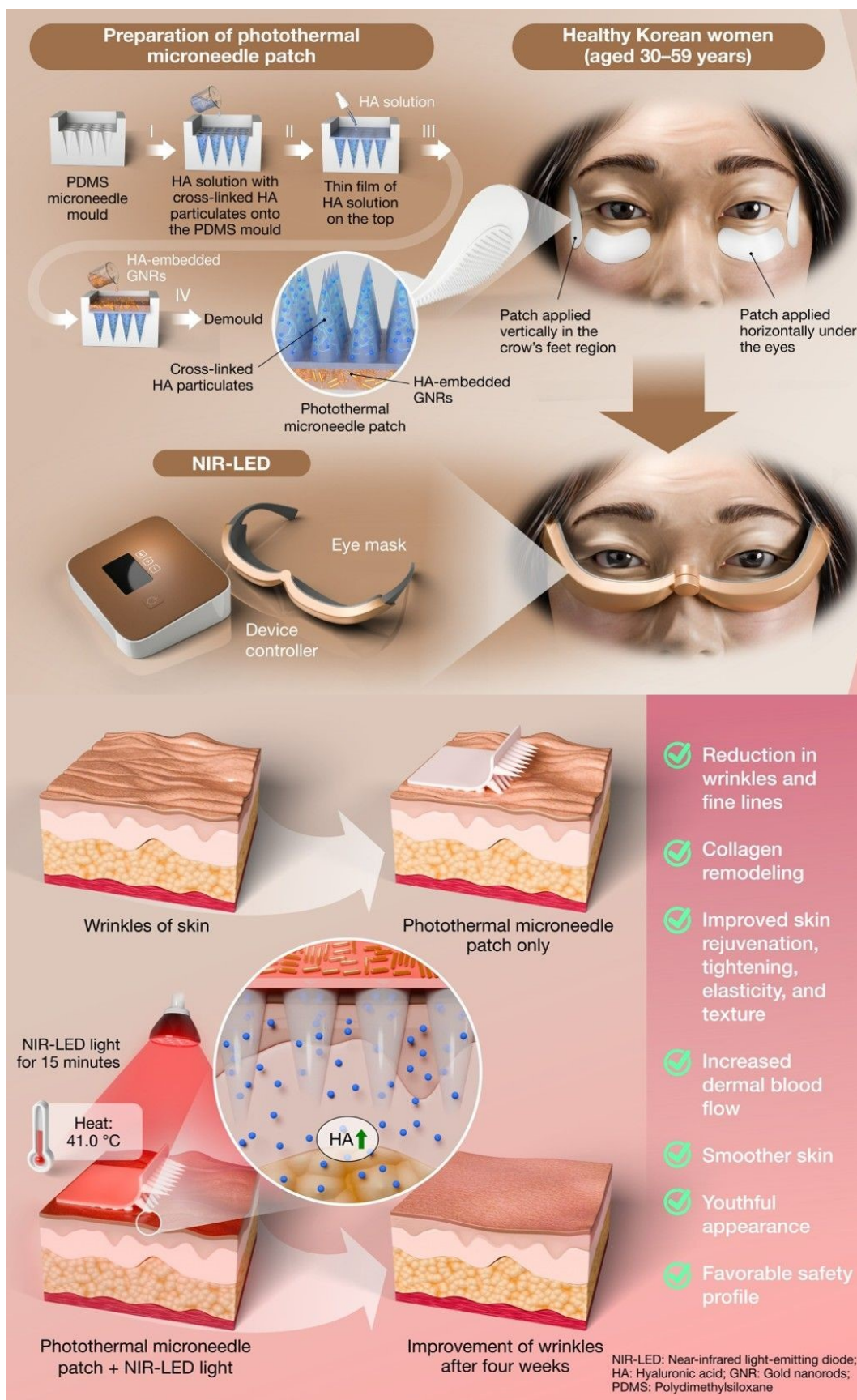
## 221 **3. Results and discussion**

### 222 **3.1. Design and fabrication of a PMP**

223 In this study, we developed the first PT-responsive soluble microneedle patch (PMP) as a novel emerging  
224 at-home cosmetic product for improving periorbital wrinkles (**Scheme 1**). The fabrication of PMP  
225 combines microneedle technology with PT materials used in medical-adhesive bandages. These PMPs  
226 were fabricated using a micromolding technique that contained cross-linked HA particulate-based needle

227 tips and an adhesive back surface of a hydrocolloid pad containing HA-GNRs (**Fig. S1**). This topology  
228 deliberately decouples penetration from actuation: the HA tips ensure painless entry into the upper  
229 epidermis, whereas the HA–GNR backing supplies heat without increasing needle length. Localizing Au  
230 to the backing (confirmed by EDX) minimizes direct metal–tissue contact while maximizing areal heat  
231 transfer to the microneedle–stratum corneum interface.





233 **Scheme 1.** Photothermal-responsive soluble microneedle eye patch (PMP) and NIR activation. The patch  
234 is fabricated using a PDMS microneedle mould by loading a hyaluronic-acid (HA) solution containing  
235 cross-linked HA particulates, overcoating with a thin HA film to form dissolvable microneedle tips, and  
236 casting a backing embedded with HA–gold nanorod (GNR) complexes, followed by demoulding. In use,  
237 patches are placed at the crow’s-feet and under the eyes; a wearable eye mask delivers NIR LED light  
238 (780 nm, 15 min) to generate mild heat ( $\sim 41$  °C) in the backing, accelerating microneedle dissolution and  
239 promoting HA diffusion into the dermis. Repeated use over four weeks is illustrated to reduce wrinkles  
240 and smooth skin, consistent with pilot clinical readouts. Abbreviations: NIR-LED, near-infrared light-  
241 emitting diode; HA, hyaluronic acid; GNRs, gold nanorods; PDMS, polydimethylsiloxane.

242  
243 GNRs have attracted considerable attention as potential PT materials because of their high  
244 absorption cross-section for converting NIR light into heat.<sup>27</sup> GNRs were prepared through the widely  
245 recognized seed-mediated growth method reported in our previous work (Korean Patent “Preparation  
246 method of Au nanorod,” No: 10-1333962).<sup>27, 36-38</sup> The UV–vis–NIR spectra of the GNRs showed strong  
247 absorbance in the NIR region (700–1100 nm) with a high longitudinal surface plasmon resonance (LSPR)  
248 band at 803 nm (**Fig. S2**), which is highly suitable for PTT with NIR light.<sup>41</sup> The TEM image of the GNRs  
249 exhibited a uniform rod-like structure with an average length of  $51.3 \pm 3.1$  nm and a diameter of  $12.6 \pm$   
250  $4.8$  nm, yielding an aspect ratio of 4.07 and resulting in excellent PT properties (**Fig. S3**).<sup>42</sup>

251 The PMPs were placed horizontally under the eyes and vertically in the crow’s feet region and  
252 gently pressed for 5 s to investigate the skin penetration capability of the patches, confirming that the  
253 entire surface of the patch was in complete contact with the skin for 5 min because of the deep penetration  
254 of the needle. An NIR LED eye mask device emitting light at a wavelength of 780 nm was worn over  
255 microneedle patches, which were exposed to the NIR LED light for 15 min to generate mild heat, followed

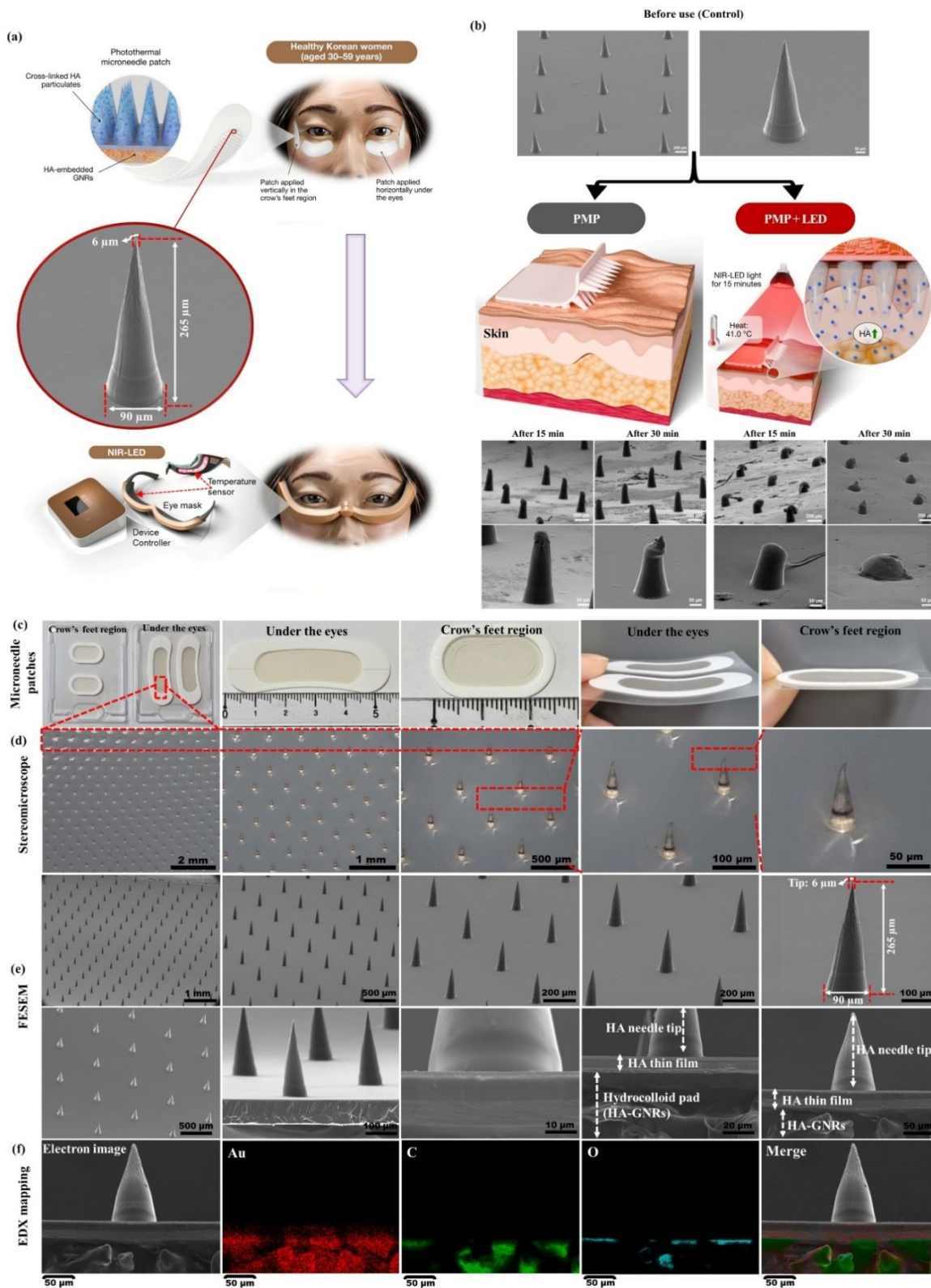


256 by cooling at room temperature without NIR LED light for 15 min, and then the NIR LED device and  
257 patches were removed. All participants were instructed to apply PMPs with NIR LED light for 15 min  
258 three times a week for a total of four weeks (**Fig. 1a**). We investigated the dissolution process of PMPs  
259 with or without NIR LED light on the skin by removing the patches at various time intervals and observing  
260 them using FESEM to confirm the patch volume changes (**Fig. 1b**). The morphology of the fabricated  
261 PMP (**Fig. 1c**) was examined using a Leica S9i stereomicroscope and FE-SEM to investigate its specificity  
262 and uniformity, particularly the average length and diameter at the base and tip. The stereomicroscopic  
263 (**Fig. 1d**) and FESEM (**Fig. 1e**) images of the fabricated PMP show a cone shape, smooth surface, and  
264 uniform array. The average length and diameter at the base and tip of the PMP were 265, 90, and 6  $\mu\text{m}$ ,  
265 respectively. The  $\sim 265 \mu\text{m}$  height targets the viable epidermis without bleeding;  $\sim 6 \mu\text{m}$  tips lower  
266 insertion force and favor rapid dissolution once hydrated, while the dense arrays (under-eye  $850 \pm 6$ ;  
267 crow's-feet  $530 \pm 5$ ) increase total heat-exchange area. The average length of 265  $\mu\text{m}$  microneedles was  
268 selected because it is painless. The total number of microneedles, strength, size, weight, and pH of the  
269 patch for periorbital wrinkles were  $850 \pm 6$ , 0.25 N, 346.4  $\text{mm}^2$ , 21 mg, and 7.1, and the total number of  
270 microneedles, strength, size, weight, and pH of the patch for the crow's feet wrinkles were  $530 \pm 5$ , 0.25  
271 N, 211.3  $\text{mm}^2$ , 14.8 mg, and 7.1, respectively. Two PMPs for periorbital wrinkles and the crow's feet  
272 region were packed into a single plastic box for ease of use during the human pilot clinical trial and applied  
273 thrice a week for a total of four weeks. Additionally, FESEM-EDX mapping was performed to visualize  
274 HA-GNRs on the adhesive back surface of the hydrocolloid pad, which indicated that Au, C, and O were  
275 uniformly distributed on the adhesive back surface of the hydrocolloid pad (**Fig. 1f**). The microneedle tips  
276 and top of the thin film of the adhesive hydrocolloid pad were in direct contact with the skin, which did  
277 not have GNRs, demonstrating that HA-GNRs were successfully fabricated on the back surface of the  
278 hydrocolloid pad. The results demonstrated that the PT microneedle tips began to dissolve after patch



279 insertion, dissolved more than three-quarters when exposed to NIR LED light for 15 min, and almost fully  
280 dissolved after 30 min of application, remaining embedded within the tissue, whereas PMPs only exhibited  
281 slight dissolution in the microneedle tip (33%) after 30 min of application (**Fig. S4**). These results confirm  
282 that NIR LED light exposure enhanced the solubility of the microneedle tips because of the PT effect of  
283 the GNRs. Additionally, the PT microneedle tip penetration depth was ~90% of the 265  $\mu\text{m}$  length after  
284 patch attachment under the eyes and crow's feet region; the penetrating PT microneedle tip was  
285 completely dissolved by bodily fluids and PT effects for further increasing the dissolution rate after 30  
286 min of application because the short length is painless and can make contact with the surface of the skin  
287 more closely. The microchannels formed by microneedle insertion are temporary and generally reseal  
288 within a few hours owing to rapid skin barrier recovery, thereby reducing the risk of infection or prolonged  
289 skin disruption. Similar findings have been reported, which showed that the length of the microneedle tip  
290 was 280  $\mu\text{m}$  and microneedle tip penetration was ~92%<sup>43</sup>. Therefore, the recommended application time  
291 for clients using PMPs is 30 min to optimize product consumption.





293 **Fig. 1.** Application of a photothermal microneedle patch (PMP) and NIR-accelerated dissolution. (a),  
294 PMP is designed for the periorbital region. A representative FESEM image shows conical microneedles  
295 (height  $\sim 265$   $\mu\text{m}$ , base  $\sim 90$   $\mu\text{m}$ , tip radius  $\sim 6$   $\mu\text{m}$ ). Patches are placed horizontally under the eyes and  
296 vertically at the crow's-feet and irradiated using a wearable eye mask with an NIR-LED (780 nm) and  
297 temperature sensing. (b), Field-emission scanning electron micrographs of microneedles before use and  
298 after 15 or 30 min of application with or without NIR-LED irradiation. NIR-LED exposure produces mild  
299 heating ( $\sim 41$   $^{\circ}\text{C}$ ) and accelerates dissolution, yielding greater tip blunting and loss of microneedle height  
300 by 30 min than the non-irradiated control. Scale bars, 200  $\mu\text{m}$  (arrays) and 50  $\mu\text{m}$  (single needles). (c),  
301 Photographs of patches tailored for the under-eye and crow's-feet regions. (d), Stereomicroscope images  
302 showing uniform microneedle arrays with enlarged views of individual tips. (e), Field-emission SEM  
303 images of arrays and cross-sections; dissolvable HA microneedle tips ( $\sim 265$   $\mu\text{m}$  height,  $\sim 90$   $\mu\text{m}$  base,  $\sim 6$   
304  $\mu\text{m}$  tip radius) are formed on a thin HA film supported by a hydrocolloid pad containing HA-gold nanorod  
305 (HA-GNR) composites. (f), Energy-dispersive X-ray (EDX) elemental maps across a cross-section,  
306 confirming Au localization within the backing layer (from HA-GNRs) and the distribution of C and O in  
307 the HA matrix. Scale bars as indicated. Data are presented as means  $\pm$  SD ( $n = 3$  independent experiments).

### 309 3.2. Photothermal actuation and accelerated dissolution under NIR-LED irradiation

310 GNRs are excellent candidates for PTT because of their high PT conversion efficiency and PT stability,  
311 which can generate mild-to-high temperatures within a short NIR laser irradiation time.<sup>44</sup> An NIR laser  
312 (wavelength 785 nm) is considered the most suitable light source for PTT because of its advantageous  
313 characteristics, including deeper tissue penetration, low absorbance by blood, water, and biological tissues,  
314 and few adverse effects.<sup>45</sup> The PT effects generated by irradiating GNRs at different concentrations (0,  
315 0.1, 1, 5, 10, 30, 50, 75, 100, and 150 ppm of Au) with a 785 nm NIR laser at 0.8 W/cm<sup>2</sup> for 30 min

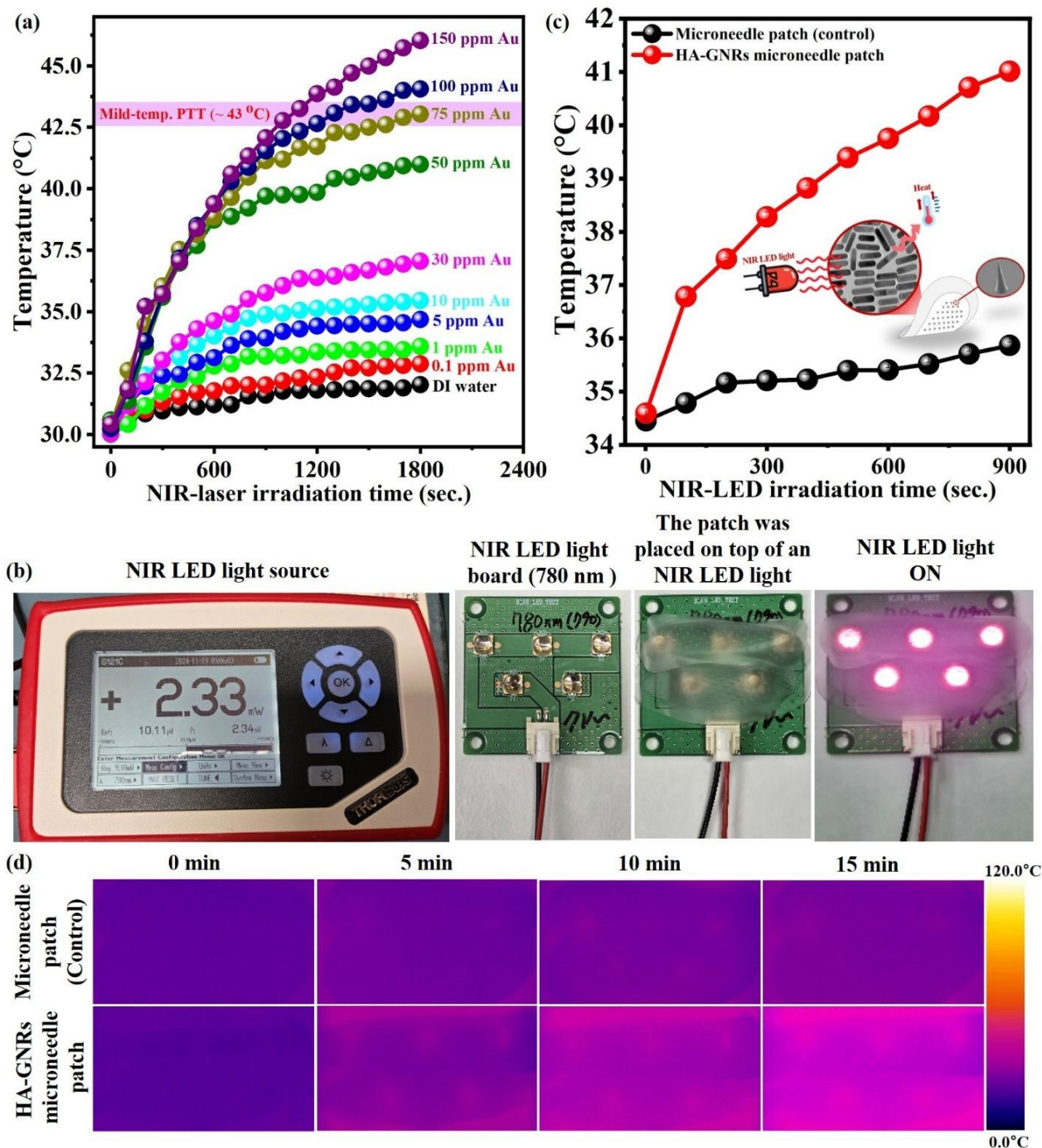
316 exhibited a concentration-dependent temperature change (**Fig. 2a**). More interestingly, the temperature of  
317 the GNRs (75 ppm of Au) quickly increased from 30.24 to 43.08 °C, where a mild temperature was more  
318 attractive and practical for PTT, whereas it only marginally increased to 32.02 °C in DW.

319 The eyelid skin is extremely sensitive to temperature changes because of its exceptionally thin and  
320 densely innervated structure. The NIR LED device controller and eye mask with a temperature sensor are  
321 used in clinical settings for managing eye protection, which provides precisely controlled heat at ~41.0 °C,  
322 indicating that the temperature is considered safe for eyelid warming.<sup>21, 46</sup> The NIR LED device was  
323 equipped with an internal surface temperature sensor integrated into a closed-loop feedback system that  
324 continuously adjusted the LED output to maintain a stable temperature of approximately 41.0 °C at the  
325 mask-patch interface. In our fabricated patches, the temperature changes in the PMPs were accurately  
326 controlled by the concentration of GNRs (75 ppm of Au). Furthermore, PMP (75 ppm of Au) and  
327 microneedle patches (0 ppm of Au) were placed on board an NIR LED light at a wavelength of 780 nm  
328 and exposed to an NIR LED light source for 15 min to investigate the PT effect of microneedle patches  
329 (**Fig. 2b**). At the patch surface, the NIR LED delivered an irradiance of 2.33 mW cm<sup>-2</sup> over an illuminated  
330 area of approximately 6.0 cm<sup>2</sup> per side, with a mask–skin distance ~ 2 mm, establishing a reproducible  
331 mild-thermal dose. The real-time temperature change curves of the PMP (75 ppm of Au) were recorded  
332 using an IR thermal imaging camera with a microneedle patch (0 ppm of Au) as a control. The temperature  
333 of the PMP (75 ppm Au) rapidly increased from 34.59 to 41.01 °C; however, the temperature of the  
334 microneedle patch only (0 ppm Au) showed a slight change from 34.45 to 35.86 °C after switching the  
335 NIR LED light on for 15 min (**Fig. 2c**). The IR thermal images of the temperature changes in the patches  
336 are shown in **Fig. 2d**. Operating near 41 °C places the system in a mild-thermal regime that (i) lowers HA  
337 viscosity at the tip–stratum corneum interface, (ii) increases water flux from the hydrocolloid, and (iii)  
338 accelerates microneedle dissolution, consistent with FESEM showing >75% tip loss at 15 min and near-



339 complete dissolution by 30 min with NIR, versus ~33% without light. During human sessions, patch-  
340 surface temperature was monitored by the mask sensor and confirmed by IR thermography, maintaining  
341 ~41 °C throughout exposure. The applied PT (~41.0 °C for 15 min) corresponds to a negligible thermal  
342 dose relative to established tissue damage thresholds (e.g., cumulative equivalent minutes at 43.0 °C  
343 (CEM43)), thereby supporting the safety of the treatment, even in sensitive periorbital skin. The PT effect  
344 rapidly increased skin temperature to ~41.0 °C, enhancing the fluidity of the epidermal lipid layer, which  
345 improved the transdermal absorption rate of anti-wrinkle agents. We hypothesized that a PMP could  
346 promote rapid heating to a skin temperature of ~41.0 °C within 15 min in human clinical trials, starting  
347 from the normal human basal body temperature (36.5–37.5 °C).





348

349 **Fig. 2.** Photothermal response of gold-nanorod-integrated microneedle patches under NIR illumination.

350 (a), Temperature-time profiles of aqueous GNR dispersions (0.1–150 ppm Au) under NIR-laser

351 irradiation (up to 1,800 s); the horizontal line marks the mild-photothermal range ( $\sim 43^\circ\text{C}$ ),

352 Experimental setup: a wearable NIR-LED light source and a 780-nm LED board; a microneedle patch

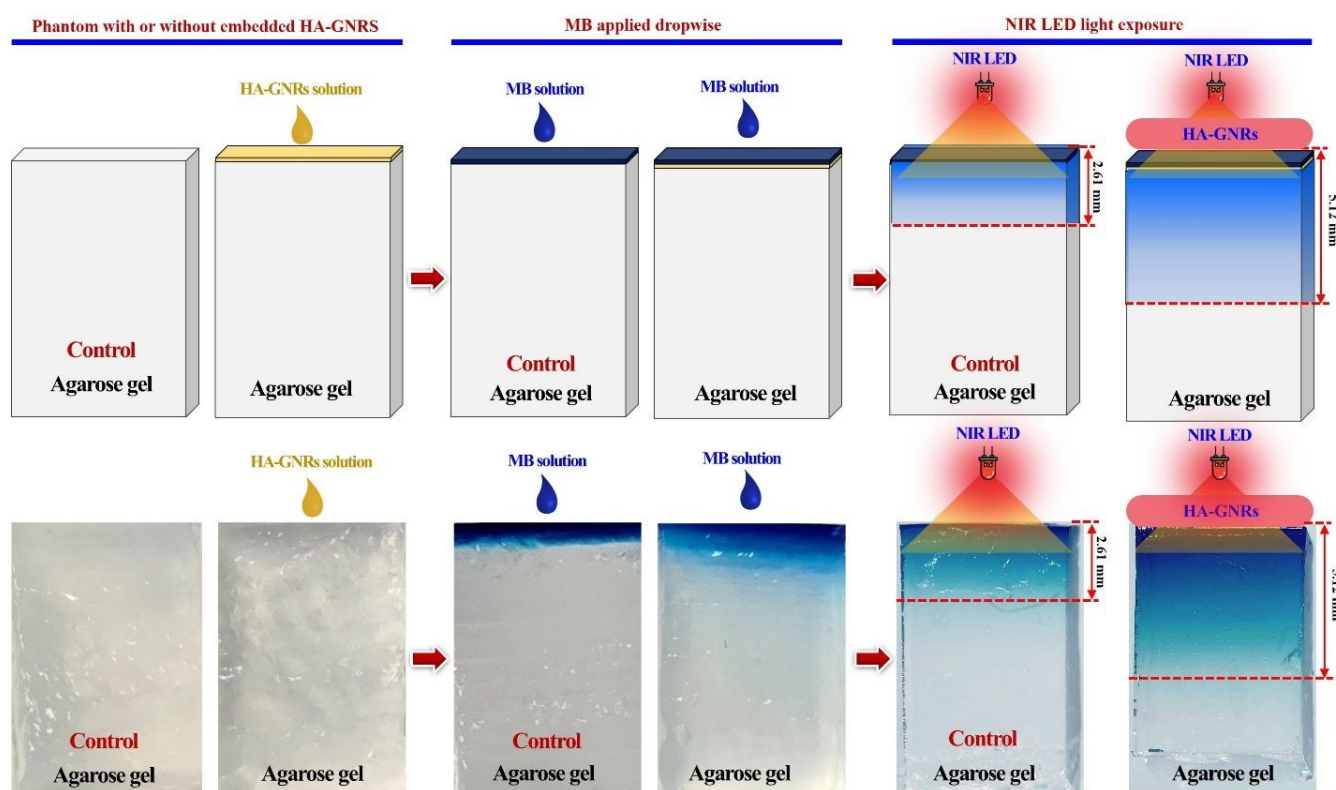


353 placed on the board and shown with the LEDs on. (c), Heating curves of the HA–GNR microneedle patch  
354 versus a control microneedle patch without GNRs during 780-nm NIR-LED irradiation for 15 min. (d),  
355 Infrared thermography at 0, 5, 10, and 15 min showing stronger warming of the HA–GNR patch relative  
356 to the control. Data are presented as means  $\pm$  SD (n = 3).

### 3.3. Tissue-phantom studies indicate deeper dye transport with NIR-activated patches

359 Biological tissue-mimicking phantoms have been proposed as artificial models to simulate biological  
360 organs and study the physicochemical impacts on the human body. The agarose gel phantom is appropriate  
361 because it mimics the target tissue and is inexpensive to prepare.<sup>47, 48</sup> MB can be used to monitor the  
362 diffusion processes occurring within an agarose gel phantom to simulate the real processes occurring in  
363 living tissues. Agarose gel phantoms were successfully created using 1% agarose powder, which was  
364 investigated for PT heat generation and diffusion (**Fig. 3**). The phantom was cylindrical and measured 7  
365 mm in diameter and 9.5 mm in height. The top of the phantom was embedded with or without HA-GNRs,  
366 and MB was applied dropwise to the top of the phantom during the diffusion. The NIR LED light (780  
367 nm) was exposed on top of the surface phantom for 15 min to visualize the depth of dye penetration in  
368 tissues because of the PT heat energy, which was measured by the MB diffusion inside the phantom. NIR-  
369 activated HA–GNR layers approximately doubled the dye-front depth ( $\approx 5.1$  mm vs  $\approx 2.6$  mm at 15 min),  
370 indicating heat-augmented diffusion/micro-convection in hydrated gels and providing a mechanistic  
371 bridge from faster on-skin dissolution to enhanced perichannel transport. Notably, this increase in  
372 penetration depth cannot be explained by thermal diffusion alone; rather, it likely arises from a  
373 combination of localized photothermal gradients, hydrogel softening, and swelling-driven  
374 microconvective transport within the hydrated matrix. The temperature increase in the gel phantom  
375 embedded with HA-GNRs and diffusion of MB into the gel phantom at a depth of dye penetration was

376 5.12 mm, indicating that the PT effect of HA-GNRs with NIR LED light can increase the molecular  
377 diffusion rate by more than two times; all molecules move because of their PT heat energy, causing  
378 diffusion. Conversely, the diffusion of MB into the gel phantom (control) with NIR LED light at the depth  
379 of dye penetration was 2.61 mm, suggesting that PT agents were absent in the control. These findings  
380 indicate that HA-GNRs exposed to NIR LED light exhibit deeper penetration of light into tissues, which  
381 is useful for clinical diagnosis.



383  
384 **Fig. 3.** Penetration depth of PT heating and dye diffusion in agarose-gel phantoms. Agarose blocks were  
385 prepared without (control) or with a surface layer containing HA-GNRs. A methylene-blue (MB) solution  
386 was applied to the top surface, and the gels were irradiated from above with an NIR LED ( $\approx 780$  nm).  
387 Schematics and photographs show that photothermal heating from HA-GNRs increased the downward

388 diffusion/convective transport of MB, shifting the visible front (red dashed line) from ~2.6 mm in the  
389 control to ~5.1 mm with HA–GNRs. Representative images from independent experiments ( $n = 3$ ).

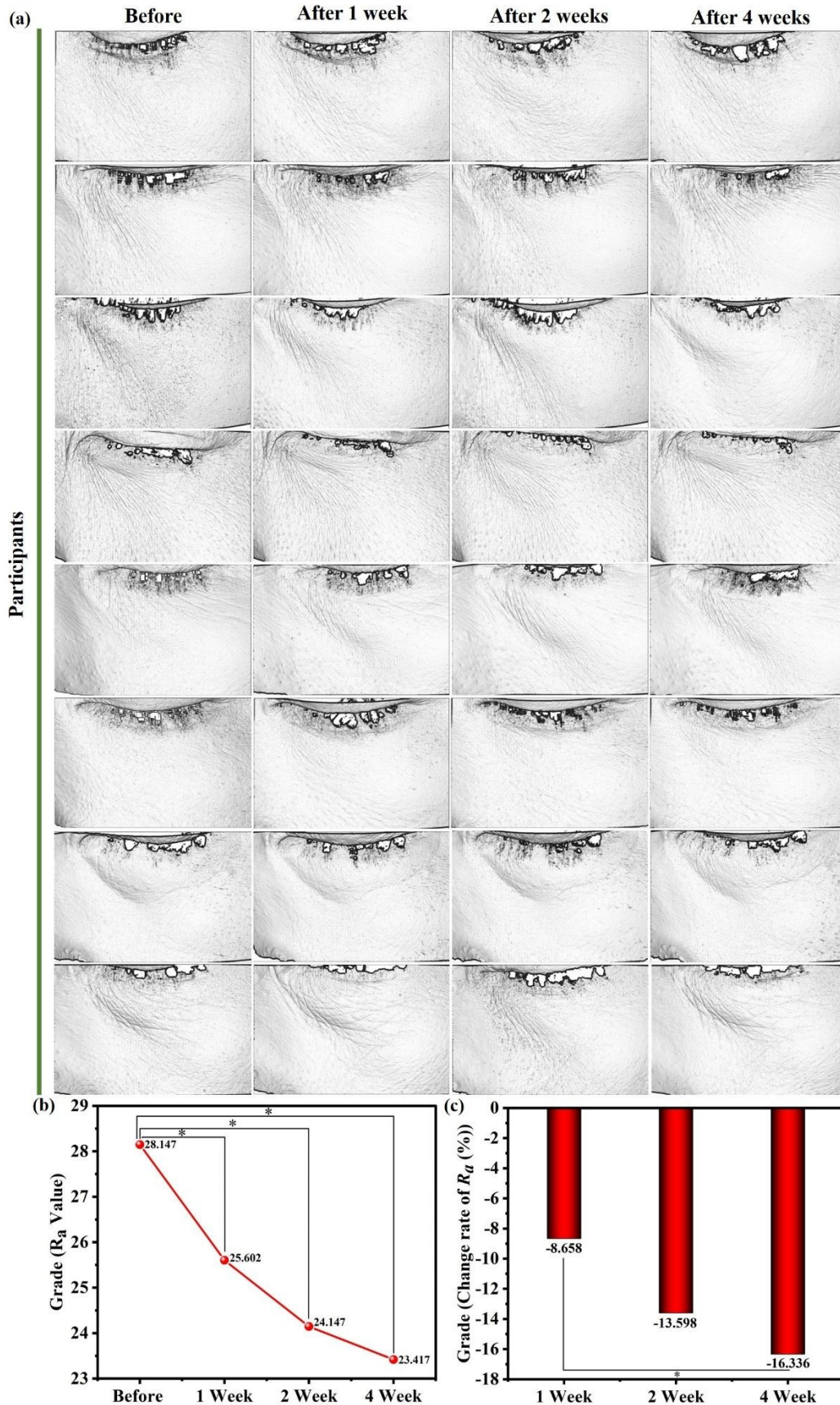
390

### 391 **3.4. Pilot randomized clinical evaluation of periorbital wrinkle reduction**

392 Twenty healthy Korean women who visited the participating clinics between November 2021 and January  
393 2022 were enrolled in the study. There were no contraindications for applying PMP in any of the  
394 participants. The average age of the 20 participants was  $50.1 \pm 6.3$  years (mean  $\pm$  SD), and all participants  
395 had mild-to-moderate periorbital wrinkles according to the modified Lemperle wrinkle assessment scale.<sup>49</sup>  
396 Furthermore, two people (10%) were in their 30s–39s, six people (30%) were in their 40s–49s, and twelve  
397 people (60%) were in their 50s–59s. A total of 20 participants completed the follow-up period and  
398 exhibited significant improvements in their periorbital wrinkles (**Fig. 4a**). Periorbital wrinkles, the crow's  
399 feet region, and skin roughness were analyzed using a small-field PRIMOS<sup>CR</sup>. The prespecified primary  
400 endpoint was percentage change in PRIMOS  $R_a$  under the eye from baseline to week 4; secondary  
401 endpoints included crow's-feet  $R_a$ , VISIA-CR L, and melanin value. **Table S1** provides information on  
402 the  $R_a$  measurements of periorbital wrinkles using PRIMOS. The  $R_a$  value was  $28.147 \pm 8.352$  prior to  
403 use. The  $R_a$  value measurement of periorbital wrinkles grading exhibited a statistically significant decrease  
404 in the first, second, and fourth weeks with a mean difference of 8.658% (Mean  $\pm$  SD:  $25.602 \pm 7.889$ ,  $p$   
405  $<0.001$ ), 13.598% (Mean  $\pm$  SD:  $24.147 \pm 7.572$ ,  $p <0.001$ ), and 16.336% (Mean  $\pm$  SD:  $23.417 \pm 7.375$ ,  $p$   
406  $<0.001$ ), respectively, indicating that the fourth week showed more improvement than other weeks (**Fig.**  
407 **4b,c**). The monotonic 8.7% $\rightarrow$ 13.6% $\rightarrow$ 16.3%  $R_a$  reductions argue against transient smoothing alone and  
408 are consistent with cumulative benefit from repeated, heat-assisted dissolution and short-range HA/water  
409 transport into microchannels. These results suggest that the PMP with NIR LED light for periorbital  
410 wrinkles improved by more than twice that of general microneedle patches. The greatest individual

411 improvement ( $\sim 50\%$  reduction in  $R_a$ ) was observed in a single participant, with a representative example  
412 shown in **Fig. 4a**, highlighting the potential efficacy of the treatment. A limitation of this experiment is  
413 the lack of a thermal control group (e.g., a simple  $\sim 41.0$  °C warm compress without GNRs). Consequently,  
414 the relative contributions of general heating and the specific PT effect of GNRs could not be fully  
415 separated. Further studies will incorporate appropriate thermal control conditions to clarify these effects.  
416





418 **Fig. 4.** Longitudinal PRIMOS assessment of periorbital wrinkles during treatment with a PMP and NIR  
419 LED. (a), PRIMOS topography images of the under-eye region from representative participants at baseline  
420 and after 1, 2, and 4 weeks of treatment with the PMP plus NIR LED (NIR-LED) irradiation, showing  
421 progressive attenuation of wrinkle features. (b), PRIMOS average roughness ( $R_a$ ) values across the same  
422 time points, indicating a steady decrease from baseline. (c), Percentage change in  $R_a$  relative to baseline  
423 at 1, 2, and 4 weeks. Statistical analysis used the Friedman test with post-hoc Wilcoxon signed-rank tests  
424 and Bonferroni correction; \* denotes corrected  $p < 0.05$ . Data are presented as means  $\pm$  SD (n = 20  
425 participants).

### 3.5. NIR-LED enhances crow's-foot outcomes versus the patch alone

428 In a with-/without-NIR comparison at the crow's-foot (ides were randomized 1:1 to PMP + NIR-LED or  
429 PMP only, with allocation concealed and PRIMOS analysis blinded to side), NIR-LED increased the mean  
430 improvement in wrinkle grade to ~14.1% at week 4 versus ~1.9% without NIR ( $\approx 7$ -fold difference), with  
431 representative PRIMOS images illustrating greater ridge attenuation under NIR-LED, matching the  
432 expected effect of faster dissolution and enhanced post-insertion transport with heating (**Fig. 5** and **Fig.**  
433 **S5**). Briefly, PMPs were applied the crow's feet region and then exposed with or without NIR LED light  
434 for 15 min (**Fig. 5**). The effect of PMP with NIR LED light in the crow's feet region was 14.1% higher  
435 than that of PMP without NIR LED light, suggesting that the effect of PMP with NIR LED light in the  
436 crow's feet region was more than seven times higher than that of the microneedle patch without NIR LED  
437 light. A 53-year-old woman with the best outcomes showed a 46% improvement in the appearance of  
438 crow's feet wrinkles (**Fig. S5**).

439

440



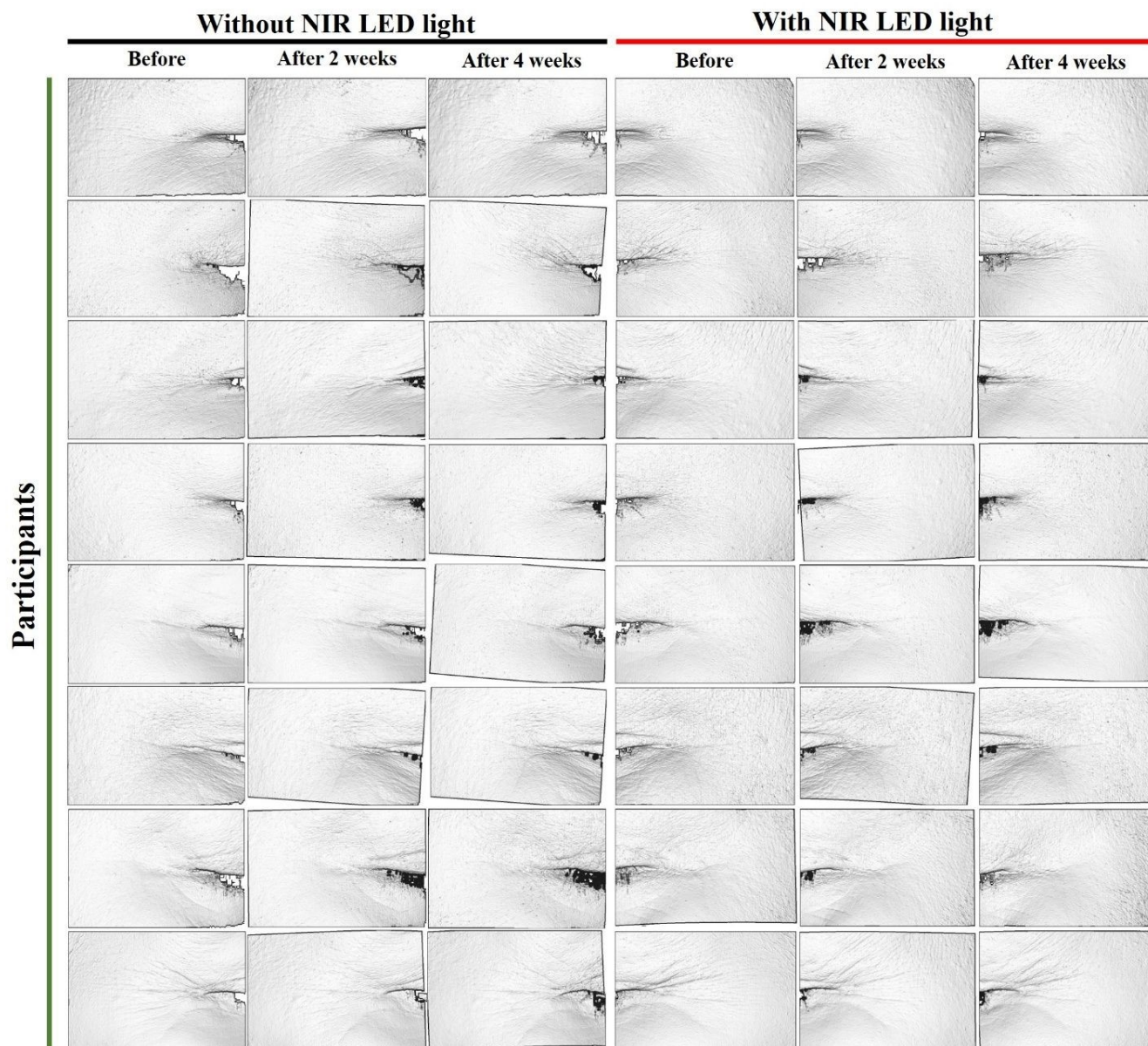


**Fig. 5.** NIR illumination enhances wrinkle improvement with a PMP. PRIMOS topography images of crow's-feet from representative participants treated with the PMP either without NIR-LED (left; baseline, week 2, week 4) or with NIR-LED (right; baseline, week 2, week 4). The addition of NIR-LED is associated with a more pronounced attenuation of wrinkle ridges over 4 weeks than PMP alone. Data are presented as means  $\pm$  SD (n = 20 participants).

441

442

443

444

445

446

447



### 448 3.6. Skin brightness increases and facial melanin decreases with NIR activation

449 Skin brightness was measured using a VISIA-CR system (**Fig. 6**). **Table S2** presents the L\* value  
450 measurements of skin brightness around the eyes using VISIA-CR. The skin brightness L\* value was  
451  $72.438 \pm 3.069$  before use, and the skin brightness L\* value was significantly increased in the first, second,  
452 and fourth weeks with a mean difference of 1.201% (Mean  $\pm$  SD:  $73.308 \pm 2.990$ ,  $p < 0.008$ ), 1.979%  
453 (Mean  $\pm$  SD:  $73.847 \pm 2.568$ ,  $p < 0.001$ ), and 1.462% (Mean  $\pm$  SD:  $73.488 \pm 3.183$ ,  $p < 0.007$ ), respectively,  
454 resulting in significantly more improvement in skin brightness (**Fig. S6a,b**). Additionally, PMPs were  
455 placed under the eyes and in the crow's feet region and exposed with or without NIR LED light for 15  
456 min (**Fig. S7**). The skin melanin changes and improvement of skin whitening effect of PMP with NIR  
457 LED light were found to be 7.29% compared to those of PMP without NIR LED light (2.83%), indicating  
458 that skin melanin-pigmented spots gradually improved the lightness of skin color from baseline (zero  
459 weeks) to four weeks for PMP with NIR LED light (**Fig. S8**). The increase in skin brightness is mainly  
460 associated with improved hydration and smoothing of the skin surface, which enhances light reflectance.  
461 The additional effect observed under NIR LED light may be related to increased local microcirculation  
462 and epidermal turnover rather than direct suppression of melanogenesis.

463 No adverse effects on the eyes or skin, such as burning, itching, scaling, prickling, redness,  
464 tightness, swelling, erythema, or edema, were reported by any participant throughout the study. No  
465 abnormal skin symptoms were detected during the physical examination by the dermatologist. In the  
466 survey of PMPs with NIR LED light preference, all participants (100%) responded "no" when asked to  
467 feel the pain and redness induced by PMPs with NIR LED light. All twenty participants completed the  
468 protocol with no device-related adverse events and no reports of pain or redness during sessions,  
469 supporting at-home feasibility with the current thermal limits. These findings indicate that PMPs irradiated  
470 with NIR LED light are safe for use in cosmetics. These findings, integrating both participant-reported

471 outcomes and dermatologist evaluations, suggest that PMP with NIR LED light treatment is well tolerated  
472 and demonstrates a favourable safety profile under the applied conditions. This study was limited by the  
473 lack of a mechanistic evaluation of wrinkle improvement. Future studies will include systematic animal  
474 experiments and histological analyses to investigate collagen remodeling, epidermal regeneration, and the  
475 associated molecular pathways induced by microneedle-assisted photothermal treatment.



**Before      After 1 week      After 2 weeks      After 4 weeks**

**Participants**



Journal of Materials Chemistry B Accepted Manuscript



477 **Fig. 6.** Representative VISIA-CR photographs showing brightening of the periorbital area during  
478 treatment. Clinical images from representative participants captured with VISIA-CR at baseline and after  
479 1, 2, and 4 weeks of treatment with the PMP plus NIR LED (NIR-LED) irradiation. The sequences  
480 illustrate progressive lightening of the under-eye region; quantitative analysis of VISIA-CR brightness  
481 ( $L^*$ ) showed a significant increase by week 2 that persisted through week 4. Data are presented as means  
482  $\pm$  SD (n = 20 participants).

#### 484 4. Conclusions

485 NIR-actuated microneedle patches combine a dissolving tip for painless penetration with a photothermal  
486 backing that supplies a repeatable, eyelid-safe thermal micro-dose, resulting in a significant reduction of  
487 wrinkles, creating smoother skin, and achieving a more youthful appearance. In this pilot trial, the system  
488 improved under-eye  $R_a$  and crow's-feet roughness and increased skin brightness, with zero device-related  
489 adverse events. Together with phantom studies showing heat-enhanced transport, the data support a  
490 mechanism in which mild heating ( $\sim 41$  °C) accelerates tip dissolution and augments short-range mobility  
491 of HA and interstitial water through combined diffusion, hydrogel softening, and micro-convective effects,  
492 producing immediate topographic smoothing.

493 Translationally, the architecture decouples penetration from actuation, allowing multiple control  
494 knobs, Au loading, LED irradiance/duty cycle, wear time, and hydrocolloid water activity to tailor thermal  
495 dose without altering needle geometry. Reporting irradiance and thermal dose will enable cross-study  
496 comparison and model-based optimization. The same platform could deliver other hydrophilic actives (for  
497 example, peptides) or pair with closed-loop temperature control using the existing mask sensor to  
498 personalize heating by skin type.

499 Future trials should (i) incorporate dose–response arms (Au concentration and irradiance), (ii)  
500 stratify by Fitzpatrick type and age to understand responders, (iii) extend follow-up to quantify durability  
501 and rebound, and (iv) include patient-reported outcomes and quality-of-life measures aligned with  
502 cosmetic benefit. A multi-site, adequately powered study with pre-registered endpoints ( $R_a$ ,  $L^*$ , melanin)  
503 and effect sizes with 95% CIs will meet community standards for evidence and facilitate regulatory and  
504 commercial translation.

505 From a manufacturability perspective, the micromoulding plus hydrocolloid process is compatible  
506 with roll-to-roll production, and gold loadings in the tens of ppm range suggest a favorable cost and  
507 environmental footprint. Careful end-of-life handling and recycling of Au from backing laminates could  
508 further improve sustainability.

## 509 **Author contributions**

510  
511 Hyo-Won Han: Methodology, Investigation, Data curation, Formal analysis. Dong-Hwan Lee:  
512 Conceptualization, Resources, Formal analysis, Investigation. Ara Joe: Project administration, Data  
513 curation, Software, Validation. Yeong Jun Jeon: Visualization, Data curation, Formal analysis. Yu-Ra  
514 Lim: Methodology, Software, Formal analysis. Sang Bong Lee: Conceptualization, Methodology,  
515 Resources. Bum-Ho Bin: Conceptualization, Resources, Methodology, Formal analysis. JuKyung Lee:  
516 Resources, Data curation, Conceptualization, Software. Thavasyappan Thambi: Software, Investigation,  
517 Methodology, Data curation. João Conde: Supervision, Resources, Funding acquisition, Visualization,  
518 Writing – review and editing. Panchanathan Manivasagan: Conceptualization, Investigation, Writing –  
519 Original Draft. Eue-Soon Jang: Supervision, Validation, Resources, Funding acquisition, Writing – review  
520 and editing.

521



522

523 **Conflicts of interest**

524 J.C. is a co-founder and shareholder of TargTex S.A. – Targeted therapeutics for Glioblastoma Multiforme.

525 J.C. is a member of the Global Burden Disease (GBD) consortium of the Institute for Health Metrics and  
526 Evaluation (IHME), University of Washington (US), and is on the Scientific Advisory Board of Vector  
527 Bioscience Cambridge. The other authors have no conflicts of interest to declare.

528

529 **Acknowledgments**

530 E.-S.J. is incredibly grateful for the research grant from the Korean Ministry of Education, Science &  
531 Technology (RS-2016-NR018634 and RS-2026-25475964), the Korea Health Technology R&D Projects  
532 (RS-2025-02263897) through the Korea Health Industry Development Institute (KHIDI) funded by the  
533 Ministry of Health and Welfare, and the Innovative Human Resource Development for Local  
534 Intellectualization Support Program (IITP-2026-RS-2020-II201612) through the Institute of Information  
535 & Communications Technology Planning & Evaluation (IITP) funded by the Korean government (MSIT),  
536 Republic of Korea. J.C. is incredibly grateful for the research grant from the Regional Innovation System  
537 & Education (RISE) program of Gyeongsangbuk-do, Republic of Korea.

538

539 **Notes and references**

- 540 1. M. Yaar, M. S. Eller and B. A. Gilchrest, *Year*.
- 541 2. Y. Ma, C. Li, Z. Mai, J. Yang, M. Tai and G. Leng, *J. Cosmet. Dermatol.*, 2022, 21, 3496-3502.
- 542 3. Q. Qu, Z. Cui, F. Jiang and C. Liu, *J. Drug Deliv. Sci. Technol.*, 2024, 100, 106065.
- 543 4. L. Baumann, *J. Pathol.*, 2007, 211, 241-251.

- 544 5. Y. Jung, E. Kim, J. Cho, K. Suh and G. Nam, *J. Eur. Acad. Dermatol. Venereol.*, 2013, 27, e328-  
545 e332.
- 546 6. S. M. Ali and G. Yosipovitch, *Acta Derm. Venereol.*, 2013, 93.
- 547 7. J. I. Lee, S. J. Kang and H. Sun, *Arch Plast. Surg.*, 2017, 44, 340-343.
- 548 8. S. Peter and S. Mennel, *Clin. Exp. Ophthalmol.*, 2006, 34, 363-364.
- 549 9. F. Bachmann, R. Erdmann, V. Hartmann, L. Wiest and B. Rzany, *Dermatol. Surg.*, 2009, 35, 1629-  
550 1634.
- 551 10. B. J. Kim, H. J. You, I. Jung and D. W. Kim, *J. Cosmet. Dermatol.*, 2020, 19, 1307-1310.
- 552 11. A. Lucaciu, P. F. Samp, E. Hattingen, R.-I. Kestner, P. Davidova, T. Kohonen, J. Rudolph, A. Dietz,  
553 H. Steinmetz and A. Strzelczyk, *Neurol. Res. Pract.*, 2022, 4, 40.
- 554 12. A. Arepagorn, J. Meephansan, P. Sirithanabadeekul, K. Tantisantisom, S. Thongma, Y.  
555 Rayanasukha, T. Boonkoom and P. Khanchaitit, *Cosmetics*, 2024, 11, 92.
- 556 13. J. Chen, C. Liufu, W. Zhang, C. Luo, K. Fu, J. Lin, J. Liang, W. Yang, F. Song and F. Yang, *Int.*  
557 *J. Cosmetic Sci.*, 2024, 46, 209-227.
- 558 14. Z. Ismail, M. S. Affandi Yusoff and K. Hashim, *J. Dispersion Sci. Technol.*, 2009, 30, 68-71.
- 559 15. X. Zhang, W. Wang, M. Zhu and D. Yu, *J. Text. Inst.*, 2018, 109, 1536-1542.
- 560 16. S. H. Lim, W. J. Tiew, J. Zhang, P. C.-L. Ho, N. N. Kachouie and L. Kang, *Biofabrication*, 2020,  
561 12, 035003.
- 562 17. X. He, J. Sun, J. Zhuang, H. Xu, Y. Liu and D. Wu, *Dose Response*, 2019, 17, 1559325819878585.
- 563 18. M. T. McCrudden, E. McAlister, A. J. Courtenay, P. González-Vázquez, T. R. Raj Singh and R.  
564 F. Donnelly, *Exp. Dermatol.*, 2015, 24, 561-566.
- 565 19. T. T. Nguyen and J. H. Park, *Expert Opin. Drug Deliv.*, 2018, 15, 235-245.



- 566 20. Y. Cong, H. Li, A. K. Pandya, L. K. Vora, Y. Li, F. Volpe-Zanutto, A. J. Paredes, A. M. Abraham,  
567 J. Gao and E. Larrañeta, *Mater. Today Adv.*, 2025, 28, 100650.
- 568 21. F. Yu, X. Zhao, Q. Wang, Y. Niu, P. Xiao, J. Zhang, K. Fei, Y. Huang, L. Liu and P. H. Fang,  
569 *Adv. Sci.*, 2025, 2413962.
- 570 22. J. H. An, H. J. Lee, M. S. Yoon and D. H. Kim, *Ann Dermatol.*, 2019, 31, 263.
- 571 23. E. Papakonstantinou, M. Roth and G. Karakiulakis, *Dermato-endocrinol.*, 2012, 4, 253-258.
- 572 24. G. D. Prestwich, D. M. Marecak, J. F. Marecek, K. P. Vercruyssen and M. R. Ziebell, *J Control.*  
573 *Release*, 1998, 53, 93-103.
- 574 25. P. Manivasagan, S. W. Jun, N. T. P. Truong, G. Hoang, S. Mondal, M. S. Moorthy, H. Kim, T. T.  
575 V. Phan, V. H. M. Doan and C.-S. Kim, *J. Mater. Chem. B*, 2019, 7, 3811-3825.
- 576 26. Y. Cheng, Q. Chen, H. Wang, L. Zhang and J. Zhu, *Macromol. Biosci.*, 2025, e00158.
- 577 27. A. Joe, P. Manivasagan, J. K. Park, H.-W. Han, S.-H. Seo, T. Thambi, V. H. Giang Phan, S. A.  
578 Kang, J. Conde and E.-S. Jang, *ACS Nano*, 2024, 18, 19581-19596.
- 579 28. W. Zhang, L. Cai, J. Gan and Y. Zhao, *Smart Med.*, 2024, 3, e20240007.
- 580 29. S. Dong, Y. Zhang, Y. Zhang, Y. Mei, A. Sina, R. Zou and L. Niu, *J. Nanobiotechnol.*, 2024, 22,  
581 199.
- 582 30. A. Zhang, X. Jiang, B. Xiong, J. Chen, X. Liu, S. Wang, B. Li, M. Peng and W. Li, *Adv. Sci.*,  
583 2025, 12, e03698.
- 584 31. F. Yu, X. Zhao, Q. Wang, Y. Niu, P. Xiao, J. Zhang, K. Fei, Y. Huang, L. Liu and P. H. Fang,  
585 *Adv. Sci.*, 2025, 12, 2413962.
- 586 32. K. Chen, X. Sun, Y. Liu, S. Li and D. Meng, *Front. Pharmacol.*, 2025, 16, 1607210.
- 587 33. T. Peng, Y. Chen, X. Luan, W. Hu, W. Wu, B. Guo, C. Lu, C. Wu and X. Pan, *Bioact. Mater.*,  
588 2025, 45, 274-300.



- 589 34. D. Jang, J. Shim, D. M. Shin, H. Noh, S. J. Oh, J. H. Park and J. H. Lee, *Dermatol. Ther.*, 2022,  
590 35, e15732.
- 591 35. J.-T. Choi, S.-J. Park and J.-H. Park, *J. Drug Target.*, 2018, 26, 884-894.
- 592 36. N. R. Jana, L. Gearheart and C. J. Murphy, *J. Phys. Chem. B*, 2001, 105, 4065-4067.
- 593 37. H.-W. Han, A. Joe and E.-S. Jang, *J. Ind. Eng. Chem.*, 2021, 96, 202-212.
- 594 38. A. Joe, H.-W. Han, Y.-R. Lim, P. Manivasagan and E.-S. Jang, *Pharmaceutics*, 2024, 16, 284.
- 595 39. D. Pratap, R. Gautam, A. K. Shaw, Vikas and S. Soni, *ACS Appl. Nano Mater.*, 2023, 6, 21350-  
596 21358.
- 597 40. L. Vilca-Quispe, J. Alvarado-Gil, P. Quintana and J. Ordonez-Miranda, *Int. J. Thermophys.*, 2010,  
598 31, 987-997.
- 599 41. P. Manivasagan, S. W. Jun, N. T. P. Truong, G. Hoang, S. Mondal, M. S. Moorthy, H. Kim, T. T.  
600 V. Phan, V. H. M. Doan and C.-S. Kim, *J. Mater. Chem. B*, 2019, 7, 3811-3825.
- 601 42. S. Bhana, R. O'Connor, J. Johnson, J. D. Ziebarth, L. Henderson and X. Huang, *J. Colloid Interface*  
602 *Sci.*, 2016, 469, 8-16.
- 603 43. R. F. Donnelly, M. J. Garland, D. I. Morrow, K. Migalska, T. R. R. Singh, R. Majithiya and A. D.  
604 Woolfson, *J. Contr. Release*, 2010, 147, 333-341.
- 605 44. K. Jiang, D. A. Smith and A. Pinchuk, *J. Phys. Chem. C*, 2013, 117, 27073-27080.
- 606 45. P. Manivasagan, F. Khan, D. R. Dhatchayeny, S. Park, A. Joe, H.-W. Han, S.-H. Seo, T. Thambi,  
607 V. G. Phan and Y.-M. Kim, *J. Adv. Res.*, 2023, 48, 87-104.
- 608 46. S. S. Lane, H. B. DuBiner, R. J. Epstein, P. H. Ernest, J. V. Greiner, D. R. Hardten, E. J. Holland,  
609 M. A. Lemp, J. E. McDonald and D. I. Silbert, *Cornea*, 2012, 31, 396-404.
- 610 47. E. L. Madsen, M. A. Hobson, H. Shi, T. Varghese and G. R. Frank, *Phys. Med. Biol.*, 2005, 50,  
611 5597-5618.



- 612 48. M. Bauman, G. Gillies, R. Raghavan, M. Brady and C. Pedain, *Nanotechnol*, 2003, 15, 92-97.
- 613 49. G. Lemperle, R. E. Holmes and S. S. M. Lemperle, *Plast. Reconstr. Surg.*, 2001, 108, 1735-1750.
- 614



## Data availability

The supporting data for this study are provided in the supplementary information. **Supplementary Information:** Fig. S1. Fabrication of a photothermal-responsive soluble microneedle eye patch. Fig. S2. UV–vis–NIR absorption of gold nanorods and overlap with the excitation source. Fig. S3. Transmission electron microscopy (TEM) of gold nanorods. Fig. S4. Near-infrared illumination accelerates dissolution of the photothermal microneedle patch. Fig. S5. Crow's-feet wrinkle improvement with and without near-infrared illumination. Fig. S6. Brightening of the periorbital skin during treatment with a photothermal microneedle patch and near-infrared LED. Fig. S7. Reduction of facial pigmentation with a photothermal microneedle patch, with and without near-infrared illumination. Fig. S8. Reduction in facial melanin with a photothermal microneedle patch, with and without near-infrared illumination. Table S1. Measure the results of wrinkles around the eyes using PRIMOS. Table S2. Measure the results of skin brightness using VISIA-CR.

